GEOPHYSICS, VOL. 71, NO. 2 (MARCH-APRIL 2006); P. K37–K45, 9 FIGS.
10.1190/1.2187768

Numerical simulation of antenna transmission and reception for crosshole ground-penetrating radar

James D. Irving[1] and Rosemary J. Knight[1]

ABSTRACT

Numerical models that account for realistic transmitter and receiver antenna behavior are necessary to develop waveform-based inversion methods for crosshole ground-penetrating radar (GPR) data. A challenge in developing such models is simulating the antennae in a computationally efficient manner so that inversions can be performed in a reasonable amount of time. We present an approach to efficiently simulate crosshole GPR transmission and reception in heterogeneous media. The core of our approach is a finite-difference time-domain (FDTD) solution of Maxwell's equations in 2D cylindrical coordinates. First, we determine the behavior of the current on a realistic GPR antenna in a borehole through detailed FDTD modeling of the antenna and its immediate surroundings. To model transmission and reception, we then replicate this antenna current behavior on a much-coarser grid using a superposition of point-electric-dipole source and receiver responses. Results obtained with our technique agree with analytical results, with numerical modeling results where the transmitter antenna and borehole are explicitly accounted for using a fine discretization, and with crosshole GPR field data.

INTRODUCTION

Over the past decade, crosshole ground-penetrating radar (GPR) has gained increasing popularity as a tool for high-resolution imaging of the shallow subsurface. Applications of this technique include delineation of ore bodies (Fullagar et al., 2000); location of underground tunnels and voids (Olhoeft, 1988; Moran and Greenfield, 1993); mapping fractures in bedrock (Olsson et al., 1992; Day-Lewis et al., 2003); and estimation of subsurface lithology and hydrogeologic properties using field- or laboratory-derived petrophysical relationships (Alumbaugh and Chang, 2002; Moysey and Knight, 2004; Tronicke et al. 2004). Of interest in our research is the use of tomographic images obtained from crosshole GPR data in the development of subsurface hydrogeologic models.

Crosshole GPR tomography is identical in principle to crosswell seismic tomography. A transmitter antenna, moved to numerous locations in one borehole, radiates high-frequency electromagnetic (EM) pulses that are recorded by a receiver antenna, which is moved down a second borehole. Most commonly, inversion of the resulting data is accomplished by assuming that the propagating radar energy can be modeled by infinite-frequency rays that join the centers of the antennae. Under this assumption, the first-break traveltimes and amplitudes of the data can be used to determine the distribution of subsurface EM-wave velocity and attenuation. The resulting ray-based tomographic images of the subsurface, however, are limited in resolution to approximately the width of the first Fresnel zone associated with the propagating pulse bandwidth (Williamson and Worthington, 1993). In order to improve resolution, we require modeling algorithms that account for more detailed physical aspects of the crosshole GPR experiment, such as wave propagation and antenna behavior. These algorithms can be employed in waveform-based inversion strategies that use all of the recorded data to determine subsurface properties (e.g., Pratt and Worthington, 1988; Zhou et al., 1995).

Geophysicists have presented a number of approaches for crosshole GPR modeling. None of these, however, allow for the simulation of both antenna transmission and reception in heterogeneous media. Sato and Thierbach (1991), for example, analytically modeled a crosshole GPR experiment using an expression for the current on an insulated dipole antenna derived by King and Smith (1981). Although their approach gives much insight into the effects of antenna and system parameters on recorded GPR wavelets, it requires a homogeneous medium between the boreholes and that the antennae

Manuscript received by the Editor December 31, 2004; revised manuscript received June 1, 2005; published online March 10, 2006.
[1]Stanford University, Department of Geophysics, Stanford, California 94305-2215. E-mail: jdirving@pangea.stanford.edu; rknight@pangea.stanford.edu.

be in the far field of one another. In addition, the expression that the authors used for the antenna current is invalid for the case of water-filled boreholes and is thus only suitable for modeling in the vadose zone. Holliger and Bergmann (2002), on the other hand, numerically modeled crosshole GPR using a finite-difference time-domain (FDTD) approach in 2D cylindrical coordinates. In their formulation, only the transmitter borehole was included in the model, and the antennae were simulated as point vertical electric dipoles. Ernst et al. (2005) further developed this algorithm to allow for detailed modeling of a realistic, finite-length transmitter antenna. Ellefsen and Wright (2005) employed a similar approach to examine the radiation patterns of realistic borehole GPR antennae. With these methods, much can be learned about the effects of the borehole, subsurface heterogeneity, and antenna characteristics on crosshole GPR radiation. However, only half of the antenna problem can be addressed. Explicit modeling of both the transmitter and receiver antennae and boreholes is not possible using 2D cylindrical coordinates and would require a fully 3D approach. Considering the many FDTD simulations that are necessary to forward-model a crosshole GPR data set and the numerous forward-model calculations that are required for inversion, such an approach remains too computationally intensive for most computers.

We present an algorithm to efficiently simulate crosshole GPR transmission and reception in heterogeneous media. This is accomplished using FDTD modeling in 2D cylindrical coordinates through a superposition of point-electric-dipole source and receiver responses. Our technique replicates the behavior of the antenna current in the boreholes without the need for explicit modeling of the antennae and boreholes. To begin, we develop the basis for our approach using analytical expressions for transmission and reception between dipole antennae located in a homogeneous medium. After demonstrating the approach for two simple cases where ideal antenna current distributions are assumed, we next discuss a means of determining the current distribution on a realistic GPR antenna located in an air- or water-filled borehole. Finally, we compare results obtained using our technique with analytical results, with numerical modeling results where the transmitter antenna and borehole are explicitly included in the modeling grid, and with crosshole GPR field data.

DEVELOPMENT OF THE MODELING ALGORITHM

FDTD modeling in 2D cylindrical coordinates

The core of our modeling approach is the FDTD solution of Maxwell's equations in 2D cylindrical coordinates presented by Holliger and Bergmann (2002). In this formulation, rotational symmetry about the vertical z-axis is assumed so that Maxwell's equations can be separated into the transverse electric (TE) and transverse magnetic (TM) modes, which are two sets of coupled partial-differential equations involving the (E_ϕ, H_r, H_z) and (E_r, E_z, H_ϕ) electric- and magnetic-field components, respectively. For crosshole GPR modeling where the antennae are oriented parallel to the z-axis, only the TM-mode equations are required. These are solved numerically in the time domain using a leap-frog, staggered-grid approach, which involves offsetting the electric- and magnetic-field components so that the finite-difference approximations of all partial derivatives are centered in both space and time (Yee, 1966). Stepping forward in time is accomplished by alternately updating the electric and magnetic fields. All updates are explicit. For approximate modeling of the radiation from an infinitesimal, vertical-electric dipole, a source current function is added to the update for the E_z field component at the desired spatial location. This amounts to adding the source function to the z-component of the current density term in Maxwell's equations (Buechler et al., 1995).

We locate our field components in space identically to Holliger and Bergmann (2002) to avoid singularity problems on the z-axis. We also use second-order-accurate finite-difference approximations for all derivatives, which means that 10 grid-points per minimum wavelength are needed to control numerical dispersion. We choose the time step according to the Courant numerical-stability criterion (Holliger and Bergmann, 2002). Higher-order approximations can be used for the spatial and/or temporal derivatives in our code, with a moderate increase in code complexity, in order to decrease the needed number of field points and thus reduce computing time (e.g., Bergmann et al., 1999). We implement perfectly matched layer (PML) absorbing boundaries in cylindrical coordinates to prevent reflections from the top, bottom, and right-hand side of the simulation grid (Berenger, 1994; Teixeira and Chew, 1997).

With the assumed cylindrical symmetry, the transmitter antenna and its borehole, which are centered on the z-axis, can be explicitly and accurately represented with the above approach. However, as mentioned previously, explicit modeling of both antennae and their boreholes to account for transmission and reception is impossible using 2D cylindrical coordinates and would require a fully 3D approach. Next, we describe how this basic code can be adopted to model both antennae transmission and reception using a superposition of point source and receiver responses.

Simulation of antenna transmission and reception

Borehole GPR antennae are generally center-fed, linear dipoles. We begin with the far-field analytical expressions for radiation and reception between two such antennae aligned parallel to the z-axis and located in a homogeneous medium. A schematic of this situation is shown in Figure 1. Both antennae have half-length l and are terminated by loads having impedance Z_0. The transmitter antenna is excited by the generator voltage pulse $V_g(t)$. Electromagnetic waves incident upon the receiver antenna induce the voltage V_r in the receiver load. In the far field, the frequency-domain expression for the radiated electric field is (Sato and Thierbach, 1991)

$$E_\theta(r, \theta, \omega) = -i\xi k \frac{e^{-ikr}}{4\pi r} h_{eff}(\omega)\, I(0, \omega), \qquad (1)$$

where r and θ are defined in Figure 1; E_θ is the total electric field in the direction of unit vector $\hat{\theta}$; ω is angular frequency; ξ and k are the electromagnetic impedance and wavenumber in the surrounding medium, respectively; $I(0, \omega)$ is the frequency-domain antenna current at the feed point $z = 0$; and $h_{eff}(\omega)$ is the θ component of the vector antenna effective

height, given by (Sengupta and Tai, 1976)

$$h_{eff}(\omega) = -\frac{\sin\theta}{I(0,\omega)} \int_{-l}^{l} I(z,\omega)\, e^{ikz\cos\theta} dz. \tag{2}$$

The parameters ξ and k are given in terms of the dielectric permittivity ϵ, magnetic permeability μ, and electrical conductivity σ, of the surrounding medium as follows:

$$\xi = \sqrt{\frac{\mu}{\epsilon - i\sigma/\omega}}, \tag{3}$$

$$k = \omega\sqrt{\mu(\epsilon - i\sigma/\omega)}. \tag{4}$$

Substituting equation 2 into equation 1, we obtain

$$E_\theta(r,\theta,\omega) = \int_{-l}^{l} \left[-i\xi k\, \frac{e^{-ikr}}{4\pi r} I(z,\omega)\sin\theta\right] e^{ikz\cos\theta} dz. \tag{5}$$

The term in brackets in equation 5 is the far-field response of an infinitesimal vertical electric dipole having current $I(z,\omega)$ (e.g., Balanis, 1997). Thus, this equation shows that the electric field radiated by the transmitter antenna could be approximated by a superposition of the responses of a number of infinitesimal electric dipoles located along the length of the antenna, each excited by some current function $I(z,t)$. This fact is used by Arcone (1995) to numerically examine the radiation patterns of resistively loaded dipoles. The delay in phase by the exponential term outside the brackets in equation 5 accounts for the differences in path length between the far-field measurement point and different points on the antenna.

Consider now the frequency-domain current at the transmitter feed point, which is related to the generator voltage as follows (Sato and Thierbach, 1991):

$$I(0,\omega) = \frac{V_g(\omega)}{Z_0 + Z_{in}(\omega)}, \tag{6}$$

where $Z_{in}(\omega)$ is the antenna input impedance. Defining

$$A(z,\omega) = \frac{I(z,\omega)}{I(0,\omega)} \left(\frac{1}{Z_0 + Z_{in}(\omega)}\right), \tag{7}$$

we have

$$I(z,\omega) = A(z,\omega)\, V_g(\omega), \tag{8}$$

or in the time domain

$$I(z,t) = A(z,t) * V_g(t). \tag{9}$$

Here, we see that the current at each point on the transmitter antenna can be expressed as the convolution of the generator voltage pulse with the function $A(z,t)$. We call $A(z,t)$ the antenna current impulse response because it represents the current that results on the antenna in response to a delta-voltage excitation.

As an example, we calculated $A(z,t)$ using the inverse Fourier transform of equation 7 for the case of a 2-m-long, bare-wire dipole antenna attached to a 50 Ω load and embedded in a lossless medium having dielectric constant $\kappa = 9$ (Figure 2). For the antenna current and input impedance, we used the familiar standing-wave expressions (e.g., Smith, 2001)

$$I(z,\omega) = I(0,\omega)\, \frac{\sin k(l - |z|)}{\sin kl} \tag{10}$$

and

$$Z_{in} = -i\, Z_c \cot kl, \tag{11}$$

which are obtained by approximating the antenna as a short-circuited transmission line having characteristic impedance Z_c. For the wavenumber on the antenna, we used the low-loss expression

$$k = \frac{\omega\sqrt{\kappa}}{c} \tag{12}$$

where c is the velocity of light in free space. We set $Z_c = 150\ \Omega$ to yield a feed-point reflection coefficient of 0.5. Figure 2 shows that, in response to an input voltage pulse, a current pulse is created on each arm of the transmitter antenna. These two pulses travel back and forth between the antenna feed and end points. For this simple example, we assumed that the velocity of the current pulses on the antenna was the same as that of the external medium. In addition, the pulses were assumed to travel without any distortion and become reduced in amplitude only upon reflection at the feed point. In the next section, we evaluate the suitability of assuming this type of simple current behavior for the crosshole GPR case.

At the receiver antenna, we are interested in an expression for V_r, the voltage induced in the receiver load by the radiated electric field. In the far field, this is given in the frequency domain by (Sato and Thierbach, 1991)

$$V_r(r,\theta,\omega) = -E_\theta(r,\theta,\omega) h_{eff}(\omega) \left(\frac{Z_0}{Z_0 + Z_{in}(\omega)}\right). \tag{13}$$

Substituting equation 2 for the effective height of the antenna into the above expression and using our definition for $A(z,\omega)$, we obtain:

$$V_r(r,\theta,\omega) = \int_{-l}^{l} [E_\theta(r,\theta,\omega)\sin\theta\, e^{ikz\cos\theta}]\, A(z,\omega) Z_0\, dz, \tag{14}$$

where integration is now along the length of the receiver antenna. The term in brackets in equation 14 is simply the z-component of the electric field at location z on the antenna.

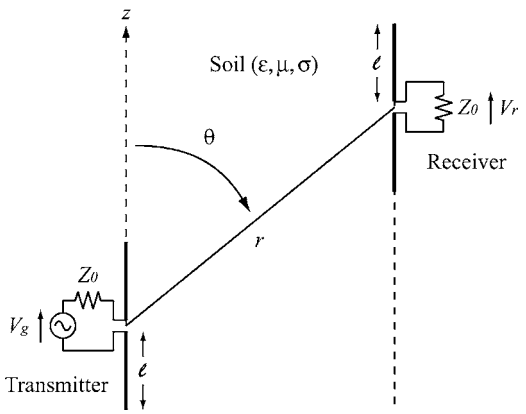

Figure 1. Basic schematic of a crosshole GPR experiment. For simplicity, the boreholes and antenna cross-sectional details have not been included. (Sato and Thierbach 1991).

Defining this quantity as $E_z(z, \omega)$, we obtain in the time domain

$$V_r(r, \theta, t) = \int_{-l}^{l} [E_z(z, t) * A(z, t)] Z_0 \, dz. \qquad (15)$$

Equation 15 shows that, similar to the transmission case, the voltage induced in the receiver load also can be approximated as a superposition of the responses of infinitesimal elements along the receiver antenna. Specifically, we can obtain $V_r(t)$ by summing the convolution of $E_z(z, t)$ and $A(z, t)$ along the antenna and multiplying this result by the load impedance Z_0. Intuitively, this can be understood as follows: At each point on the receiver antenna, the E_z component of the incident EM pulse from the transmitter antenna induces current pulses that travel in both directions away from that point. As in the transmission case, these pulses reverberate along the antenna arm. Just as $A(z, t)$ describes how an impulsive voltage at the transmitter antenna feed is related to the current experienced at each point along the antenna, it also describes how an impulsive voltage excitation at each point on the receiver antenna is related to the current experienced at the center. Thus, we convolve $E_z(z, t)$ with $A(z, t)$ and sum along the antenna to obtain the total current in the receiver load. The multiplication by Z_0 transforms this current into voltage.

Based on the above results, we can numerically simulate crosshole GPR transmission and reception using the previously described FDTD code in 2D cylindrical coordinates. To model transmission, we first obtain the antenna current distribution by convolving the excitation voltage pulse with $A(z, t)$. To the update for the E_z field at each point in the simulation grid corresponding to a location on the transmitter antenna, we then add the appropriate current function, which simulates infinitesimal vertical electric dipole radiation from that point. Together, the responses of the infinitesimal dipoles emulate the radiation of the finite-length antenna. To model reception, the E_z field at all nodes collocated with the receiver antenna is stored during the finite-difference simulation. After the time stepping is complete, the recorded data are convolved with the appropriate values of $A(z, t)$ and then summed and multiplied by Z_0 to obtain the receiver load voltage.

In simulating transmission and reception in this manner, we avoid explicit, detailed modeling of the antennae and their boreholes, and instead account for these features through the antenna current behavior. As a result, we can perform modeling very efficiently on a relatively coarse grid. In addition, although we used far-field expressions to derive this approach, we are not restricted to the far field, and the approach is thus perfectly valid for the small borehole separations that are typically encountered in crosshole GPR.

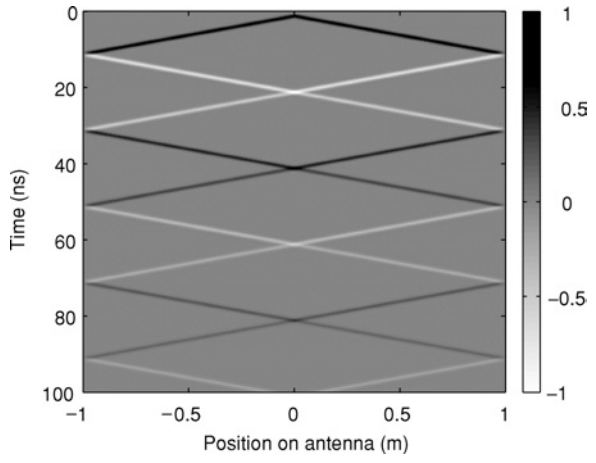

Figure 2. Normalized antenna current impulse response, $A(z, t)$, for a 2-m-long, bare-wire, standing-wave dipole antenna embedded in a lossless $\kappa = 9$ medium. Results were obtained using the inverse Fourier transform of equation 7.

Examples for standing-wave and Wu-King dipole antennae

As basic examples of our modeling approach, Figures 3 and 4 show the radiated E_z field and receiver load voltage determined for two cases that represent the end members of commercial borehole GPR antennae. In Figure 3, we used the antenna current impulse response function from Figure 2 to model radiation and reception between 2-m-long, standing-wave dipole antennae embedded in a lossless, homogeneous

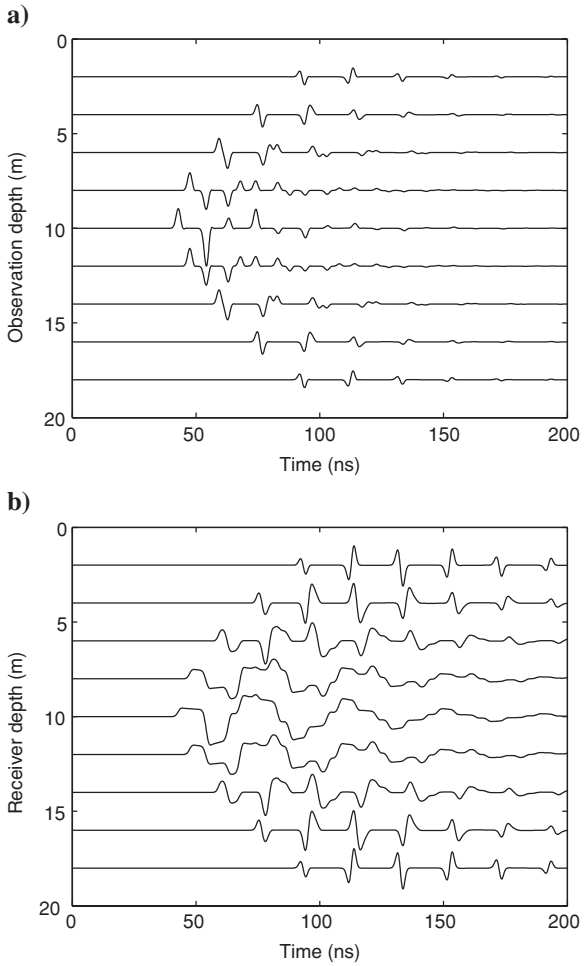

Figure 3. (a) Radiated E_z field and (b) received waveform determined for 2-m-long, standing-wave dipole antennae in a lossless $\kappa = 9$ medium.

medium having $\kappa = 9$. The transmitter antenna was placed at a depth of 10 m, and the horizontal antenna separation was 4 m. For the excitation voltage, we used a Gaussian pulse, given by

$$V_g(t) = \exp\left[-\left(\frac{t - t_0}{\tau}\right)^2\right], \tag{16}$$

where the characteristic time τ was set equal to 1 ns, and t_0 was chosen such that $V_g(0)$ is the first point in the Gaussian where the amplitude reaches 0.1% of its maximum value. Notice that the radiated E_z field for the standing-wave dipole consists of a series of positive and negative pulses, each of which represents radiation from either the antenna feed or end points in accordance with time-domain antenna theory (Smith, 1997; Smith, 2001). That is, although we have superimposed the responses of infinitesimal dipoles along the entire length of the antenna to model the radiated wavefield, these responses cancel everywhere on the dipole except at the feed and end points, where charge acceleration and deceleration take place. We purposely chose a short excitation pulse and long antennae for this example to demonstrate this effect. If the antennae were shortened, the current pulse velocity along the antennae were increased, or the excitation pulse were lengthened, then the discrete arrivals seen in Figure 3 would merge. This typically occurs in crosshole radar data (Sato and Thierbach, 1991). There is also a significant difference between the E_z and received voltage waveforms in Figure 3. Whereas the E_z waveform consists of distinct pulses in time, the received waveform appears more like an integrated pulse sequence. This is also in accordance with time-domain antenna theory (Shlivinski et al., 1997; Smith, 2004), and illustrates the importance of properly accounting for reception, in addition to transmission, when modeling crosshole GPR data.

In Figure 4, we used the same modeling parameters and experimental geometry as Figure 3, but altered $A(z, t)$ to simulate transmission and reception between resistively loaded, Wu-King dipole antennae (Wu and King, 1964). Specifically, the amplitude of the original standing-wave dipole impulse response shown in Figure 2 was linearly tapered to zero at the ends of the antenna so that (Smith, 1997)

$$A_{wk}(z, t) = \begin{cases} A_s(z, t)\{1 - |z|/l\} & \text{if } t \le l/v_{ant}, \\ 0 \text{ otherwise}, \end{cases} \tag{17}$$

where v_{ant} is the velocity of the current pulses on the antenna, $A_{wk}(z, t)$ is the Wu-King dipole impulse response, and $A_s(z, t)$ is the standing-wave dipole impulse response. Whereas a standing-wave antenna sustains pulses of current that travel back and forth along the antenna arms, a Wu-King dipole is loaded with resistance in such a manner as to be reflectionless. For this reason, the pulses of current on a Wu-King dipole travel only from the feed point to the ends of the antenna before they decay to zero amplitude. Figure 4 shows that, in contrast to the standing-wave case, the radiated and received waveforms for the Wu-King dipole are very compact. Because there are no reflections on the antenna, radiation comes largely as an initial pulse from the feed point (Smith, 1997). The results in Figure 4 are in accordance with those of Sengupta and Liu (1974), who analytically investigated the response of Wu-King dipoles to Gaussian pulse excitation.

In practice, commercial borehole GPR antennae lie somewhere between the undamped, standing-wave dipoles of Figure 3 and the Wu-King dipoles of Figure 4. That is, these antennae tend to be lightly resistively loaded to achieve a compromise between power radiated into the ground and pulse width, which ideally should be short. Indeed, crosshole GPR waveforms that we have recorded in the field tend to contain more peaks and troughs than the waveforms displayed in Figure 4b but significantly less of these than the waveforms shown in Figure 3b.

Behavior of the antenna current for crosshole GPR

To model antenna transmission and reception using a superposition of point source and receiver responses, we require prior knowledge of the antenna current behavior, contained in $A(z, t)$. For the examples in Figures 3 and 4, ideal $A(z, t)$ functions were assumed. In using these functions, the velocity of the current pulses on the antennae was assumed to be the same as the EM-wave velocity of the surrounding medium, and the pulses were assumed to undergo no change in shape as they traveled along the antenna arms. For the simple case

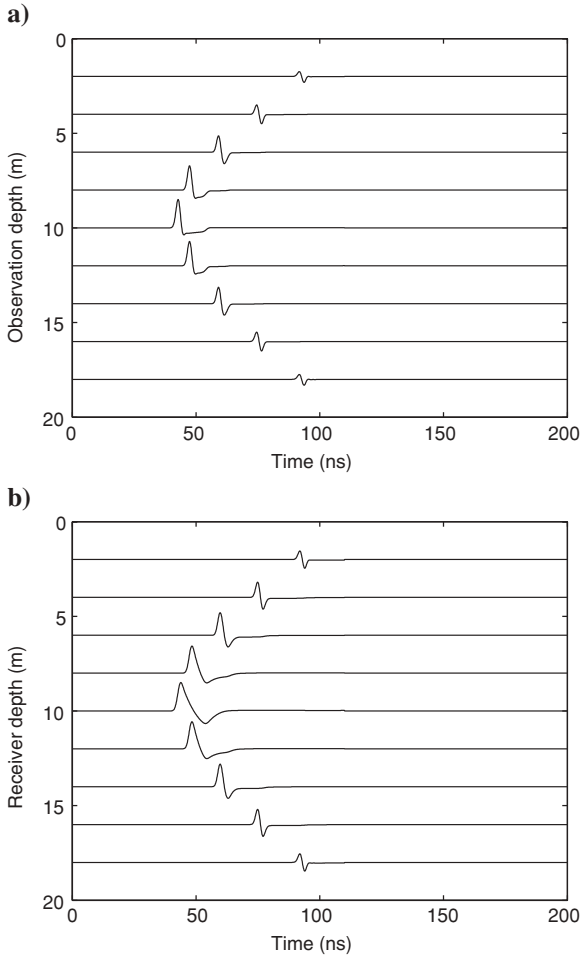

Figure 4. (a) Radiated E_z field and (b) received waveform determined for 2-m-long, resistively loaded (Wu-King) dipole antennae in a lossless, $\kappa = 9$ medium.

of a thin, bare-wire antenna embedded in a homogeneous medium, this behavior may be a reasonable approximation to reality (Balanis, 1997). However, in the crosshole radar case, the antennae are insulated and located in air- or water-filled boreholes. As a result, such simple $A(z, t)$ functions are generally invalid.

In the situation where the materials between the antenna wire and the external medium (i.e., the antenna insulation and borehole-filling material for the crosshole GPR case) have significantly lower dielectric permittivities than the external medium, a realistic current distribution on an insulated antenna may be obtained analytically (King and Smith, 1981; King et al., 1983). Under these conditions, the antenna can be treated as a short-circuited transmission line and characterized by equations 10 and 11, but with a characteristic impedance that is complex and frequency-dependent and a wave number different from that of the surrounding medium. Sato and Thierbach (1991) use these results in their analytical formulation of crosshole GPR transmission and reception. However, as mentioned previously, this approach is valid only for modeling in the vadose zone, as in the saturated zone, the material present in the borehole (water) has a significantly higher dielectric permittivity than the surrounding earth.

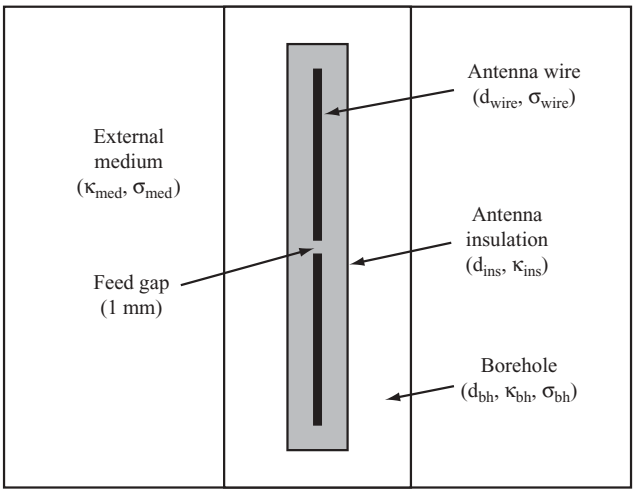

Figure 5. Modeling domain used to determine the behavior of the current on a realistic borehole GPR antenna.

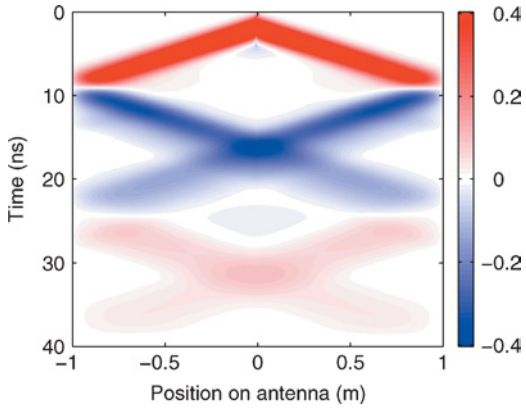

Figure 6. Normalized transmitter antenna current for an insulated, 2-m-long, dipole antenna located in a 5-cm-diameter, air-filled borehole and surrounded by earth having $\kappa_{med} = 9$ and $\sigma_{med} = 1$ mS/m. Results were determined using a finely discretized FDTD simulation with the outer boundary set 0.5 m away from the antenna axis.

To determine realistic current behavior for crosshole GPR antennae in both air- and water-filled boreholes, without any assumptions or approximations, we use a detailed FDTD modeling approach in 2D cylindrical coordinates. In a similar manner to Ernst et al. (2005) and Ellefsen and Wright (2005), we model explicitly the transmitter antenna and borehole, using a fine spatial discretization. We then simulate transmission on the antenna and examine the current distribution. To reduce computing time, we limit the extent of our model to a small region around the borehole. Figure 5 shows the modeling domain that we consider for this approach. The antenna wire, with diameter d_{wire} and electrical conductivity σ_{wire}, contains a small, 1-mm feed gap at the center. The wire is surrounded by lossless insulation having external diameter d_{ins} and dielectric constant κ_{ins}. The borehole, with diameter d_{bh}, is characterized by either $\kappa_{bh} = 1$ and $\sigma_{bh} = 0$ mS/m (air-filled) or $\kappa_{bh} = 80$ and $\sigma_{bh} = 1$ mS/m (water-filled). The surrounding medium has electrical properties κ_{med} and σ_{med}. For all materials, we assume that the magnetic permeability equals its free space value, μ_0. To feed the antenna and represent the correct impedance contrast at the input terminals, we attach a 1D transmission line that is terminated at the far end with an absorbing boundary condition (Maloney et al., 1994; Lampe et al., 2003). The voltage excitation function is then introduced into the line through a one-way injector. To obtain the current on the antenna from the FDTD modeling results, we apply the integral formulation of Ampere's Law to the H_ϕ field nodes located just outside the antenna wire.

Figure 6 shows the antenna current that we obtained using this approach for a 2-m-long, insulated dipole located in a 5-cm-diameter, air-filled borehole and excited by a Gaussian pulse with $\tau = 1$ ns. This borehole diameter is typical

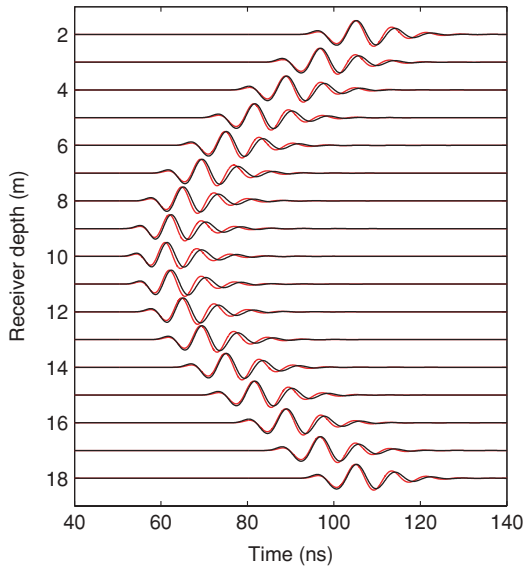

Figure 7. Comparison of received waveforms computed using our approach (black) and determined analytically using the method of Sato and Thierbach (1991) (red).

of the PVC-cased piezometer wells that we commonly use for our crosshole GPR work. The surrounding earth had $\kappa_{med} = 9$ and $\sigma_{med} = 1$ mS/m. The antenna wire was modeled as a copper cylinder with $d_{wire} = 5$ mm and $\sigma_{wire} = 5 \times 10^7$ S/m. For the insulation, we used $d_{ins} = 30$ mm and $\kappa_{ins} = 4$. These specifications approximately model the cross-section of our commercial borehole GPR antennae. The characteristic impedance of the 1D feeding transmission line was set to 50 Ω. Figure 6 shows, as described previously, that a pulse of current travels back and forth on each arm of the antenna in response to the excitation voltage pulse. In contrast to the simple cases considered earlier, however, these pulses undergo significant broadening as they propagate because of the presence of the antenna insulation and borehole. This shows that we cannot ignore dispersion that occurs along the antennae when modeling crosshole GPR. For the case of a water-filled borehole, the dispersion was found to be even more significant than we show here. Also important in Figure 6 is the fact that the velocity of the current pulses on the antenna is 0.14 m/ns, which is significantly greater than the EM-wave velocity of the surrounding earth (approximately 0.1 m/ns). Clearly, the antenna insulation and borehole have a marked effect on the antenna current distribution, and thus, on transmission and reception.

To model crosshole GPR using our approach, the actual current on the antennae is not required, but rather, the antenna current impulse response $A(z, t)$. However, FDTD modeling using a true impulse voltage excitation to obtain $A(z, t)$ would require an extremely fine spatial discretization because of the high frequency components involved and the fact that 10 grid points per minimum wavelength are required to control numerical dispersion. To obtain a reasonable approximation to $A(z, t)$ for our purposes, we compute the antenna current as described above using a Gaussian excitation pulse whose frequency spectrum is essentially white over the bandwidth of the transmitter excitation pulse of interest. We have found that setting $\tau = 0.1$ ns in equation 16 yields a good approximation to $A(z, t)$ for crosshole GPR modeling. In addition, we have found that $A(z, t)$ is relatively insensitive to moderate fluctuations in the electrical properties of the earth surrounding the antennae; that is, the antenna current behavior is much more dependent upon the properties of the insulation and material filling the borehole. As a result, we often need to compute $A(z, t)$ only once, using an average value for the earth's electrical properties, to adequately model an entire crosshole GPR survey.

COMPARISON WITH ANALYTICAL, NUMERICAL, AND FIELD RESULTS

To validate our modeling approach, we now compare results obtained using our code with analytical results, numerical modeling results where the transmitter antenna and borehole have been explicitly discretized, and crosshole GPR field data. For all cases, 0.8-m-long dipole antennae were considered, which is the length of the frequently employed 100-MHz center frequency antennae in our crosshole GPR system. The transmitter antenna for all cases was located at 10 m depth, and the antenna wire was assumed to be a 5-mm-diameter copper cylinder. A Gaussian excitation pulse with $\tau = 2$ ns (e.g., Sato and Thierbach, 1991) was used for all of the simulations. We believe this is a close approximation to the voltage pulse delivered by our commercial system transmitter. We normalized each trace in the gathers presented below by the maximum value in order to allow an easier comparison of the individual waveforms, whose amplitudes decrease sig-

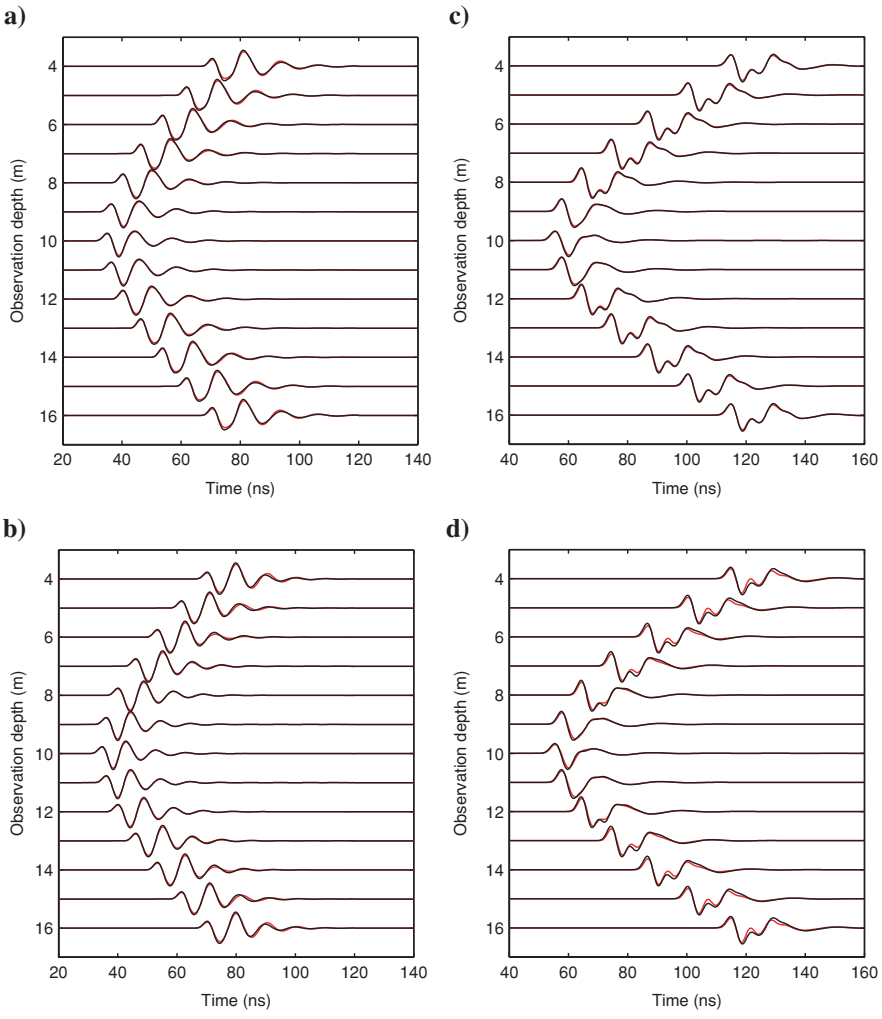

Figure 8. Comparison of radiated E_z field computed using our approach (black) and using a finely discretized FDTD code with the transmitter antenna and borehole explicitly modeled (red). (a) vadose zone, 5-cm-diameter borehole; and (b) vadose zone, 10-cm-diameter borehole; (c) saturated zone, 5-cm-diameter borehole; and (d) saturated zone, 10-cm-diameter borehole.

nificantly at high propagation angles. In each case, the absolute amplitudes of the data being compared were in excellent agreement.

Figure 7 compares the receiver load waveforms obtained using our code with the analytical results of Sato and Thierbach (Sato and Thierbach, 1991) for the case where the antennae were situated in 5-cm-diameter, air-filled boreholes and surrounded by a homogeneous medium having $\kappa_{med} = 9$ and $\sigma_{med} = 1$ mS/m. For this example, the borehole separation was 5 m. The modeled antennae were not insulated (i.e., $d_{ins} = d_{wire}$) because the formulation presented by Sato and Thierbach considers only one material between the antenna wire and the surrounding earth. Their approach could be extended to include both the antenna insulation and borehole-filling material using the results of King et al. (1983). As seen in Figure 7, there is excellent agreement between our results and the analytical solution.

In Figure 8, we compare the radiated E_z field determined using our approach, with that obtained by explicitly modeling the transmitter antenna and its borehole using a very fine spatial discretization in a similar manner to Ernst et al. (2005) and Ellefsen and Wright (2005). We examined four cases which represent 5-cm- and 10-cm-diameter boreholes in vadose- and saturated-zone environments. In all of these cases, the insulated antenna profile used for Figure 6 was employed. The E_z field was recorded at points along a vertical line 3 m away from the transmitter borehole. In the vadose-zone examples (Figures 8a and 8b), the borehole was air-filled and surrounded by a homogeneous medium having $\kappa_{med} = 9$ and $\sigma_{med} = 1$ mS/m. Here, we see that our results are nearly identical to those determined through detailed FDTD modeling. In the saturated zone examples (Figures 8c and 8d), the borehole was filled with water, and the surrounding medium had $\kappa_{med} = 25$ and $\sigma_{med} = 5$ mS/m. Again, the results obtained using the two approaches are in excellent agreement. Clearly, in accounting for the transmitter antenna and borehole by replicating the antenna current behavior on a significantly coarser grid, we are able to accurately obtain the radiated wavefield.

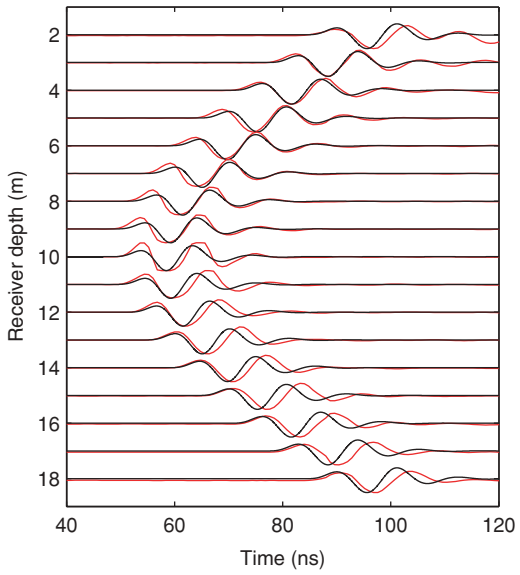

Figure 9. Comparison of received waveforms modeled using our approach (black) and recorded in the field in an unsaturated sand-and-gravel aquifer deposit (red).

Recent work shows that, in addition to affecting the current distribution on an antenna, a water-filled borehole may distort antenna radiation through guided-wave effects (Holliger and Bergmann, 2002; Tronicke et al., 2004; Tronicke and Holliger, 2004). Indeed, there is slightly less agreement between our code and the detailed modeling results for the 10-cm-diameter, water-filled borehole case shown in Figure 8d, which we believe is related to this phenomenon. Although the differences between our code and the finely discretized results in Figure 8d are minor, it is important to emphasize that our methodology can only account for guided-wave effects to the extent that they affect the antenna current distribution. For some combinations of antenna excitation pulse and borehole diameter in water-filled boreholes, it is possible that guided-wave effects that cannot be modeled with our approach may be more significant than we show here.

As a final example, Figure 9 compares results obtained using our code with crosshole GPR field data collected between 5-cm-diameter, air-filled piezometer wells located in a relatively homogeneous, unsaturated, glaciofluvial sand-and-gravel deposit near Abbotsford, British Columbia, Canada. The boreholes were 6 m apart. Again, we modeled the antennae using the insulated antenna profile from Figure 6. In addition, to obtain the best match with the field data, we included constant resistive loading along the antennae. This was accomplished by increasing the resistivity of the antenna wire cells in the detailed FDTD simulation that was used to obtain $A(z, t)$. We used an average value of $\kappa_{med} = 6$, which was obtained from picked first-arrival times in the crosshole data. We estimated the conductivity of the sand and gravel to be 1 mS/m. Figure 9 shows our modeling results and the field data to be in good agreement. The received waveforms are very similar, except for a slightly broader received pulse in the field data, especially at high angles (i.e., longer travel paths), which we suspect is related to intrinsic dispersion in the sand and gravel. We have not accounted for frequency-dependent material properties in our FDTD code, but including dispersion into the algorithm would be straightforward (e.g., Bergmann et al., 1998).

CONCLUSIONS

Through a relatively simple modification of the FDTD algorithm of Holliger and Bergmann (2002), we can simulate both antenna transmission and reception for crosshole GPR in heterogeneous media. A significant advantage of our approach is that modeling can be performed very efficiently on a relatively coarse, 2D grid. In addition, our method allows us to simulate the current behavior on realistic borehole GPR antennae very accurately because we obtain $A(z, t)$ from a detailed FDTD simulation where the antenna and borehole features are included explicitly. Our next step is to use this modeling approach to develop a full-waveform inversion strategy for crosshole GPR data. Although it has been shown recently that guided-wave effects may significantly affect antenna radiation in water-filled boreholes, our method was able to model radiation in both 5-cm- and 10-cm-diameters water-filled boreholes very accurately. However, some combinations of borehole diameter and transmitter excitation pulse may

produce guided-wave effects that cannot be completely accounted for through the antenna current distribution. If these effects are determined to be important, they could at least be partly accounted for with our code by explicitly modeling the transmitter borehole. Finally, it is likely that our formulation could also be used, with a few modifications, to model transmission and reception in a vertical radar profile (VRP) configuration. This is a topic of future research.

ACKNOWLEDGMENTS

This research was supported by funding to R. Knight from the National Science Foundation, Grant Number EAR-0229896-002. J. Irving was also supported during this work through a Departmental Chair's Fellowship at Stanford University. We thank reviewers Steve Arcone, Klaus Holliger, and associate editor Joe Dellinger for suggestions that improved this manuscript.

REFERENCES

Alumbaugh, D., and P. Y. Chang, 2002, Estimating moisture contents in the vadose zone using cross-borehole ground-penetrating radar: A study of accuracy and repeatability: Water Resources Research, **38**, 1309, doi:10.1029/2001WR000754.

Arcone, S. A., 1995, Numerical studies of the radiation patterns of resistively loaded dipoles: Journal of Applied Geophysics, **33**, 39–52.

Balanis, C. A., 1997, Antenna theory: Analysis and design: Harper & Row.

Berenger, J. P., 1994, A perfectly matched layer for the absorption of electromagnetic waves: Journal of Computational Physics, **114**, 185–200.

Bergmann, T., J. O. Blanch, J. O. A. Robertsson, and K. Holliger, 1999, A simplified Lax-Wendroff correction for staggered-grid FDTD modeling of electromagnetic wave propagation in frequency-dependent media: Geophysics, **64**, 1369–1377.

Bergmann, T., J. O. A. Robertsson, and K. Holliger, 1998, Finite-difference modeling of electromagnetic wave propagation in dispersive and attenuating media: Geophysics, **63**, 856–867.

Buechler, D. N., D. H. Roper, C. H. Durney, and D. A. Christensen, 1995, Modeling sources in the FDTD formulation and their use in quantifying source and boundary condition errors: IEEE Transactions on Microwave Theory and Techniques, **43**, 810–814.

Day-Lewis, F. D., J. W. Lane, J. M. Harris, and S. M. Gorelick, 2003, Time-lapse imaging of saline tracer transport in fractured rock using difference radar attenuation tomography: Water Resources Research, **39**, 1290, doi:10.1029/2002WR001722.

Ellefsen, K. J., and D. L. Wright, 2005, Radiation pattern of a borehole radar antenna: Geophysics, **70**, K1–K11.

Ernst, J. R., K. Holliger, and H. Maurer, 2005, Realistic FDTD modelling of borehole georadar antenna radiation: Methodology and application: Near Surface Geophysics, SEG.

Fullagar, P. K., D. W. Livelybrooks, P. Zhang, and A. J. Calvert, 2000, Radio tomography and borehole radar delineation of the McConnell nickel sulphide deposit, Sudbury, Ontario, Canada: Geophysics, **65**, 1920–1930.

Holliger, K., and T. Bergmann, 2002, Numerical modeling of borehole georadar data: Geophysics, **67**, 1249–1257.

King, R. W. P., and G. S. Smith, 1981, Antennas in matter: Fundamentals, theory, and applications: MIT Press.

King, R. W. P., B. S. Trembly, and J. W. Strohbehn, 1983, The electromagnetic field of an insulated antenna in a conducting or dielectric medium: IEEE Transactions on Microwave Theory and Techniques, **MTT-31**, 574–583.

Lampe, B., K. Holliger, and A. G. Green, 2003, A finite-difference time-domain simulation tool for ground-penetrating radar antennas: Geophysics, **68**, 971–987.

Maloney, J. G., K. L. Shlager, and G. S. Smith, 1994, A simple FDTD model for transient excitation of antennas by transmission lines: IEEE Transactions on Antennas and Propagation, **42**, 289–292.

Moran, M. L., and R. J. Greenfield, 1993, Radar signature of a 2.5-D tunnel: Geophysics, **58**, 1573–1587.

Moysey, S., and R. J. Knight, 2004, Modeling the field-scale relationship between dielectric constant and water content in heterogeneous systems: Water Resources Research, **40**, W03510, doi:10.1029/2003WR002589.

Olhoeft, G. R., 1988, Interpretation of hole-to-hole radar measurements: 3rd Symposium on Tunnel Detection, Proceedings, 616–629.

Olsson, O., L. Falk, O. Forslund, L. Lundmark, and E. Sandberg, 1992, Borehole radar applied to the characterization of hydraulically conductive fracture zones in crystalline rock: Geophysical Prospecting, **40**, 104–116.

Pratt, R. G., and M. H. Worthington, 1988, The application of diffraction tomography to cross-hole seismic data: Geophysics, **53**, 1284–1294.

Sato, M., and R. Thierbach, 1991, Analysis of a borehole radar in cross-hole mode: IEEE Transactions on Geoscience and Remote Sensing, **29**, 899–904.

Sengupta, D. L., and Y. Liu, 1974, Analytical investigation of waveforms radiated by a resistively loaded linear antenna excited by a Gaussian pulse: Radio Science, **6**, 621–630.

Sengupta, D. L., and C. T. Tai, 1976, Radiation and reception of transients by linear antennas, *in* L. B. Felsen, ed., Transient electromagnetic fields: Springer.

Shlivinski, A., E. Heyman, and R. Kastner, 1997, Antenna characterization in the time domain: IEEE Transactions on Antennas and Propagation, **45**, 1140–1149.

Smith, G. S., 1997, An introduction to classical electromagnetic radiation: Cambridge University Press.

———, 2001, Teaching antenna radiation from a time-domain perspective: Americal Journal of Physics, **69**, 288–300.

———, 2004, A direct derivation of a single-antenna reciprocity relation for the time domain: IEEE Transactions on Antennas and Propagation, **52**, 1568–1577.

Teixeira, F. L., and W. C. Chew, 1997, Systematic derivation of anisotropic PML absorbing media in cylindrical and spherical coordinates: IEEE Microwave and Guided Wave Letters, **7**, 371–373.

Tronicke, J., and K. Holliger, 2004, Effects of gas- and water-filled boreholes on the amplitudes of crosshole georadar data as inferred from experimental evidence: Geophysics, **69**, 1255–1260.

Tronicke, J., K. Holliger, W. Barrash, and M. D. Knoll, 2004, Multivariate analysis of cross-hole georadar velocity and attenuation tomograms for aquifer zonation: Water Resources Research, **40**, W01519, doi:10.1029/2003WR002031.

Williamson, P. R., and M. H. Worthington, 1993, Resolution limits in ray tomography due to wave behaviour: Geophysics, **58**, 727–735.

Wu, T. T., and R. W. P. King, 1964, The cylindrical antenna with nonreflecting resistive loading: IEEE Transactions on Antennas and Propagation, **AP-12**, 369–373.

Yee, K. S., 1966, Numerical solution of initial boundary value problems involving Maxwell's equations in isotropic media: IEEE Transactions on Antennas and Propagation, **14**, 302–307.

Zhou, C., W. Cai, Y. Luo, G. Schuster, and S. Hassanzadeh, 1995, Acoustic wave-equation traveltime and waveform inversion of crosshole seismic data: Geophysics, **60**, 765–773.